Manuscript prepared for Atmos. Chem. Phys.
with version 2015/09/17 7.94 Copernicus papers of the LaTeX class copernicus.cls.
Date: 20 May 2016

Dimethyl sulfide in the summertime Arctic atmosphere: Measurements and source sensitivity simulations

Emma L. Mungall[1], Betty Croft[2], Martine Lizotte[3], Jennie L. Thomas[4], Jennifer G. Murphy[1], Maurice Levasseur[3], Randall V. Martin[2], Jeremy J. B. Wentzell[5], John Liggio[5], and Jonathan P. D. Abbatt[1]

[1]Department of Chemistry, University of Toronto, Toronto, Canada
[2]Department of Physics and Atmospheric Science, Dalhousie University, Halifax, Canada
[3]Québec-Océan, Department of Biology, Université Laval, Québec, Canada
[4]Sorbonne Universités, UPMC Univ. Paris 06, Université Versailles St-Quentin, CNRS/INSU, LATMOS-IPSL, Paris, France
[5]Air Quality Processes Research Section, Environment Canada, Toronto, Ontario, Canada

Correspondence to: Jon Abbatt (jabbatt@chem.utoronto.ca)

Abstract. Dimethyl sulfide (DMS) plays a major role in the global sulfur cycle. In addition, its atmospheric oxidation products contribute to the formation and growth of atmospheric aerosol particles, thereby influencing cloud condensation nuclei (CCN) populations and thus cloud formation. The pristine summertime Arctic atmosphere is strongly influenced by DMS. However, atmospheric DMS mixing ratios have only rarely been measured in the summertime Arctic. During July-August, 2014, we conducted the first high time resolution (10 Hz) DMS mixing ratio measurements for the Eastern Canadian Archipelago and Baffin Bay as one component of the Network on Climate and Aerosols: Addressing Key Uncertainties in Remote Canadian Environments (NETCARE). DMS mixing ratios ranged from below the detection limit of 4 pptv to 1155 pptv (median 186 pptv) during the 21-day shipboard campaign. A transfer velocity parameterization from the literature coupled with coincident atmospheric and seawater DMS measurements yielded air-sea DMS flux estimates ranging from 0.02-12 μmol m^{-2}d^{-1}. Air-mass trajectory analysis using FLEXPART-WRF and sensitivity simulations with the GEOS-Chem chemical transport model indicated that local sources (Lancaster Sound and Baffin Bay) were the dominant contributors to the DMS measured along the 21-day ship track, with episodic transport from the Hudson Bay System. After adjusting GEOS-Chem oceanic DMS values in the region to match measurements, GEOS-Chem reproduced the major features of the measured time series, but was biased low overall (2-1006 pptv, median 72 pptv), although within the range of uncertainty of the seawater DMS source. However, during some 1-2 day periods the model under predicted the measurements by more than an order of magnitude. Sensitivity tests indicated that non-marine sources (lakes, biomass burning, melt ponds and coastal tundra) could make additional episodic contributions to atmospheric DMS in the study region, although local marine sources of DMS dominated. Our results highlight the need for both atmospheric and seawater DMS

datasets with greater spatial and temporal resolution, combined with further investigation of non-marine DMS sources for the Arctic.

1 Introduction

Despite the established importance of oceanic emissions of biogenic sulfur in the form of dimethyl sulfide (DMS) to aerosol formation and growth in the marine boundary layer (e.g. Charlson et al., 1987; Leaitch et al., 2013), key uncertainties remain about oceanic DMS concentrations and the air-sea flux of DMS (Tesdal et al., 2015). DMS emissions are responsible for about 15% of the tropospheric sulfur budget globally, and up to 100% in some remote areas (Bates et al., 1992). Due to its low solubility and high volatility (small Henry's Law constant) and its supersaturation in the ocean with respect to the atmosphere, DMS partitions to the atmosphere after being produced by micro-organisms in surface waters. In the atmosphere, DMS is oxidized to sulfuric acid and methane sulfonic acid (MSA). These oxidation products can then participate in new particle formation (Pirjola et al., 1999; Chen et al., 2015) or condense upon existing particles, causing them to grow larger and changing particle hygroscopicity. The influence of DMS emissions on aerosol concentrations is important since aerosols modify the climate directly by scattering and absorbing radiation, and indirectly by modifying cloud radiative properties by acting as seeds for cloud droplet formation (Charlson et al., 1987; Twomey, 1977; Albrecht, 1989). Both composition and size affect the ability of an aerosol particle to act as a cloud condensation nucleus (CCN), with bigger and more hygroscopic aerosol particles preferentially activating as CCN (K ohler, 1936).

The summer Arctic atmosphere contains very few CCN through a combination of limited local sources and efficient scavenging mechanisms (Browse et al., 2012). At low CCN levels the radiative balance as determined by cloud cover is very sensitive to CCN number (Carslaw et al., 2013). Sea ice cover in the summer Arctic is in rapid decline (e.g. Tilling et al., 2015). With the decline in sea ice comes an enhanced potential for sea-air exchange of compounds such as DMS that may affect aerosol populations in the Arctic. In general, increased numbers of CCN are associated with a cooling effect on climate. However, portions of the Arctic can reside in a CCN-limited cloud-aerosol regime, with the result that an increase in CCN could have a warming effect due to increases in cloudiness in turn increasing the trapping of outgoing long-wave radiation (Mauritsen et al., 2011). In order to predict future changes in CCN number, we need to understand the influence of sea-air exchange on summertime Arctic aerosols.

Quantifying present-day atmospheric DMS mixing ratios (henceforth referred to as DMS_g) provides an important benchmark for interpreting future measurements. Currently, only a few snapshots of DMS_g in the Arctic exist from a handful of ship-board studies conducted over the last twenty years, none of which captured the most biologically productive time of June and July (Leck and Persson, 1996; Rempillo et al., 2011; Chang et al., 2011; Tjernström et al., 2014). The data span

great distances in time and space and provide only a fragmented picture of tropospheric DMS_g levels in the Arctic. Understanding present-day sources of DMS_g is also relevant for predicting how these sources may change in a future climate.

The lifetime of DMS_g against OH oxidation of 1-2 days suggests that DMS_g may either undergo long-range transport before being oxidized or remain in the same area under low wind conditions. Atmospheric transport mixes DMS_g within a region, effectively smoothing out atmospheric concentration inhomogeneities due to inhomogeneity in the surface water DMS (referred to henceforth as DMS_{sw}). Transport can also bring DMS_g from regions further afield. For example, a study by Nilsson and Leck (2002) highlighted the importance of transport in bringing DMS_g from regions of open water to regions covered by sea ice within the Arctic.

Despite the potential for an important role for atmospheric transport, few source apportionment studies for sulfur in the Arctic have been carried out. Previous work has focused almost exclusively on the aerosol phase. Methane sulfonic acid (MSA) in the aerosol phase is commonly assumed to arise from oxidation of marine biogenic DMS_g (Sharma et al., 2012). However, Hopke et al. (1995) suggested that terrestrial sources in Northern Canada could also contribute MSA to Arctic aerosol. Previous studies indicate that terrestrial emissions of DMS_g from soils, vegetation, wetlands and lakes are less important than oceanic emissions (Bates et al., 1992; Watts, 2000). However, these studies are based on very few or even no measurements in the Canadian North, and the fluxes for the Canadian tundra and boreal forest, which cover a very large surface area, are highly unconstrained. Much of the Arctic Ocean is in close proximity to land and is more subject to terrestrial influence than the open ocean in other regions of the world (Macdonald et al., 2015).

Sources of DMS_g other than seawater are not typically included in chemical transport and climate models, despite evidence for several other sources of DMS_g. For example, significant levels of DMS have been measured in Canadian lakes (Sharma et al., 1999a; Richards et al., 1994). DMS emissions have also been observed from various continental sources such as lichens (Gries et al., 1994), crops such as corn (Bates et al., 1992), wetlands (Nriagu et al., 1987), and biomass burning (Meinardi et al., 2003; Akagi et al., 2011). Terrestrial plants can be an important source of DMS as demonstrated by DMS levels in the hundreds of pptv range measured from creosote bush in Arizona and from trees and soils in the Amazonian rain forest (Jardine et al., 2010, 2014). One previous study based on sulfur isotopes from Greenland included a pooled biogenic continental and volcanic source (as the isotopic signatures of these two sources are not easily distinguishable) and estimated this continental component to be 44% (Patris et al., 2002). In addition to the possibility of a continental source, melt ponds have been suggested as a potentially important source of DMS to the atmosphere (Levasseur, 2013). These fresh or brackish ponds form from snow melt on top of the sea ice in spring and summer, and have been observed to have an extremely large areal extent, covering 30% of the sea ice on average in midsummer with up to 90% coverage in some regions (Rosel and Kaleschke, 2012).

Here we present sensitivity studies to examine the potential importance of these alternative sources of DMS_g.

The goals of this study are 1) to present ship-board DMS_g measurements taken in the Canadian Arctic during July and August 2014, and 2) to explore possible sources for the measured DMS_g.

Section 2 outlines our measurement methodology. Section 3 presents the measured DMS_g time series along 3 weeks of the cruise. Section 3 also includes concurrent measurements of DMS_{sw} and the calculated DMS air-sea flux estimates for the region. Section 4 presents sensitivity studies with the GEOS-Chem chemical transport model and the FLEXPART-WRF particle dispersion model, which examine the potential contribution of seawater and non-marine sources to the measured DMS_g.

2 Methods

2.1 Measurements

Measurements of DMS were made during the first leg of the CCGS *Amundsen* summer campaign under the aegis of NETCARE (Network on Climate and Aerosols: Addressing Uncertainties in Remote Canadian Environments). The research cruise started in Quebec City on 8 July, 2014 and ended in Kugluktuk on 14 August, 2014. Measurements were made in Baffin Bay, Lancaster Sound and Nares Strait. The ship track is shown in Fig. 1a.

2.1.1 DMS mixing ratios

DMS_g measurements were made using a high resolution time of flight chemical ionization mass spectrometer (HR-ToF-CIMS, Aerodyne). The instrument was housed in a container on the foredeck. The inlet was placed on a tower 9.44 m above the deck at the bow, which was itself nominally 6.6 m above sea level (in total ca. 16 m above sea level). A diaphragm pump pulled air at 30 L min^{-1} through a 25 m long, 9.53 mm inner diameter PFA line heated to 50°C (Clayborn Labs). Flow rate through the line was controlled by a critical orifice. The flow was subsampled and pulled to the instrument inlet through another critical orifice restricting the flow to 2 L min^{-1}. The flow through the sealed ^{210}Po source of the HR-ToF-CIMS, also controlled at 2 L min^{-1} by a critical orifice, was supplied by a zero air generator (Parker Balston, Model HPZA-18000, followed by a Carbon Scrubber P/N B06-0263) via a mass flow controller supplying 2.4 L min^{-1}. The zero air generator also supplied 9.8 sccm (controlled by a mass flow controller) through a bubbler filled with benzene, which was added to the flow through the radioactive source to provide the reagent ion. The excess went to exhaust. Figure S1 shows a flow schematic.

The use of benzene cations as a reagent ion for chemical ionization mass spectrometry was first proposed by Allgood et al. (1990). This reagent ion was successfully applied to the shipboard detection of DMS_g by Kim et al. (2015). The ionization mechanism that prevails is the transfer of charge from a benzene cation to an analyte ion which has an ionization energy lower than that of benzene

(Allgood et al., 1990). Due to space constraints on board the ship, a zero air generator was used instead of cylinder nitrogen to produce our reagent ion flows. The use of zero air introduced other potential reagent ions to the mass spectrum (O_2^+, NO^+, $C_6H_7^+$, and $H_2O{\cdot}H_3O^+$, shown in Fig. S2). To investigate the effect of this more complicated reagent ion source, calibration experiments were carried out in the laboratory prior to the campaign for both air and N_2 at different sample flow relative humidities and under different CIMS voltage configurations. The calibration curves for DMS (detected as $CH_3SCH_3^+$) showed a linear response under all conditions. We found that the sensitivity of the instrument to DMS did not depend on relative humidity. The average sensitivity measured by one-point calibrations in the field (±1 σ) was 80±30 cps/pptv. Actual uncertainties on the calibration factor were less as a time-varying calibration factor was applied to the data, as described below. Detection limits were below 4 pptv as the background was consistently 2-3 pptv.

Background spectra were collected in the field by overflowing the inlet with zero air from the zero air generator as shown in Fig. S1. The high mass resolution of the instrument eliminated concern about unit mass isobaric interferences as indicated in Fig. S3. Mass spectra were collected at 10 Hz. One point calibrations were performed nearly every day by overflowing the inlet with zero air and adding a known amount of DMS from a standards cylinder using a mass flow controller (499 ±5% ppb, Apel-Reimer). Peak fitting was performed using the Tofware software package from Aerodyne (version 2.4.4) in Igor Pro. Reported mixing ratios were calculated by first normalizing analyte peak areas to reagent ion peak areas, then subtracting backgrounds, and finally applying calibration factors obtained by linearly interpolating the one-point daily calibrations. Text S1 provides details. To remove artifacts that might have occurred due to enhanced DMS flux in the ship's wake, the data were filtered such that values were removed when the ship was moving (speed over ground greater than 2 m s^{-1}) and the wind direction was not within ±90° of the bow. This filtering removed less than 12% of data points.

2.1.2 Surface seawater DMS concentrations

Seawater concentrations of DMS were determined following procedures described by Scarratt et al. (2000) and modified in Lizotte et al. (2012) using purging, cryotrapping and sulfur-specific gas chromatography. Briefly, seawater was gently collected directly from 12L Niskin bottles in gas-tight 24-ml serum vials, allowing the water to overflow. Subsamples of DMS were withdrawn from the 24-ml serum vials within minutes of collection and sparged using an in line purge and trap system with a Varian 3800 gas chromatograph (GC) equipped with a pulsed flame photometric detector (PFPD). The GC was calibrated with injections of a 100 nM solution of hydrolyzed DMSP (Research Plus Inc.). The full dataset will be presented separately [*Lizotte et al., personal communication*].

2.1.3 Meteorological data

Basic meteorological measurements were made from a purpose built tower on the ship's foredeck. Air temperature (8.2 m above deck), wind speed and direction (9.4 m above deck) and barometric pressure (1.5 m above deck) were measured using, respectively, a shielded temperature & relative humidity probe (Vaisala™HMP45C212), wind monitor (RM Young 05103) and pressure transducer (RM Young™61205V). Sensors were scanned every 2 s and saved as 2 min averages to a micrologger (Campbell Scientific™, model CR3000). Platform relative wind was post-processed to true wind following Smith et al. (1999). Navigation data (ship position, speed over ground, course over ground and heading) necessary for the conversion were available from the ship's position and orientation system (Applanix POS MV™V4). Periods when the tower sensors were serviced or when the platform relative wind was beyond ±90° from the ship's bow were screened from the meteorological data set. Screened periods accounted for less than 20% of total data but up to 45% in some regions.

2.1.4 Sea surface temperature and salinity

Sea surface temperature (SST) was measured with the ship's Inboard Shiptrack Water System, Seabird/Seapoint measurement system. There were no continuous salinity measurements. An average salinity value of 29.7 PSU was used for all calculations since the calculated transfer velocities had very low sensitivity to changes in salinity for our study region.

2.2 Model Descriptions

2.2.1 FLEXPART-WRF

A Lagrangian particle dispersion model based on FLEXPART (Stohl et al., 2005), FLEXPART-WRF (Brioude et al., 2013, website: flexpart.eu/wiki/FpLimitedareaWrf), was used to study the origin of air sampled by the ship. The model is driven by meteorology from the Weather Research and Forecasting (WRF) Model (Skamarock et al., 2005) and was run in backward mode to study the emissions source regions and transport pathways influencing ship-based DMS measurements. Specific details are in Wentworth et al. (2016).

2.2.2 GEOS-Chem

The GEOS-Chem chemical transport model (www.geos-chem.org) was used to conduct source sensitivity studies. We used GEOS-Chem version 9-02 at 2° x 2.5° resolution with 47 vertical layers between the surface and 0.01 hPa. The assimilated meteorology is taken from the National Aeronautics and Space Administration (NASA) Global Modeling and Assimilation Office (GMAO) Goddard Earth Observing System version 5.7.2 (GEOS-FP) assimilated meteorology product, which includes both hourly surface fields and 3-hourly 3D fields. Our simulations used 2014 meteorology and allowed a 2-month spin-up prior to the simulation of July and August, 2014.

The GEOS-Chem model includes a detailed oxidant-aerosol tropospheric chemistry mechanism as originally described by Bey et al. (2001). Simulated aerosol species include sulphate-nitrate-ammonium (Park et al., 2004, 2006), carbonaceous aerosols (Park et al., 2003; Liao et al., 2007), dust (Fairlie et al., 2007, 2010) and sea salt (Alexander et al., 2005). The sulphate-nitrate-ammonium chemistry uses the ISORROPIA II thermodynamic model (Fountoukis and Nenes, 2007), which partitions ammonia and nitric acid between the gas and aerosol phases. The model includes natural and anthropogenic sources of SO_2 and NH_3 (Fisher et al., 2011). DMS emissions are based on the piecewise linear Liss and Merlivat (1986) sea-air flux formulation (due to recent studies reporting a linear wind-speed dependence for DMS (Huebert et al., 2010; Bell et al., 2013, 2015)) and DMS_{sw} concentrations from Lana et al. (2011). In our simulations, DMS emissions occurred only in the fraction of the grid box that is covered by sea water and also free of sea ice. Biomass burning emissions are from the Quick Fire Emissions Dataset (QFED2) (Darmenov and da Silva, 2013), which provides daily open fire emissions at 0.1° x 0.1°. Oxidation of SO_2 occurs in clouds by reaction with H_2O_2 and O_3 and in the gas phase with OH (Alexander et al., 2009) and DMS oxidation occurs by reaction with OH and NO_3.

The GEOS-Chem model has been extensively applied to study the Arctic atmosphere, in regard to aerosol acidity (Wentworth et al., 2016; Fisher et al., 2011), carbonaceous aerosol (Wang et al., 2011), aerosol number (Croft et al., 2016), aerosol absorption (Breider et al., 2014), and mercury (Fisher et al., 2012).

2.2.3 Seawater DMS values in GEOS-Chem

The GEOS-Chem model uses the monthly mean DMS_{sw} from the climatology of Lana et al. (2011), which was developed based on data with very limited spatial coverage in the Canadian Arctic Archipelago and Baffin Bay as shown by Fig. S1 in Lana et al. (2011). In contrast, our recent DMS_{sw} measurements are spread quite evenly throughout the 21-day ship track and thus have a considerably greater spatial extent throughout our study region than the sources used for the Lana et al. (2011) climatology. The Lana et al. (2011) climatology contains maximum DMS_{sw} of 5 nM for our study region. However, the DMS_{sw} measured during our ship-board campaign was generally between 5-10 nM and occasionally higher. Therefore, we used the 35 measured DMS_{sw} values to create an updated DMS_{sw} field for use as a GEOS-Chem input in the study region. The measured values were interpolated using the DIVA web application (http://gher-diva.phys.ulg.ac.be/web-vis/diva.html) and a static field was used for July and August. The Lana et al. (2011) climatology was used for all other ocean regions. While our updated DMS_{sw} has improved spatial coverage and is a better temporal match to our study than the Lana et al. (2011) dataset, we acknowledge that there are remaining uncertainties related to spatial and temporal resolution.

To our knowledge, there are no measurements of DMS_{sw} in the Hudson Bay System (comprising Hudson Bay, Foxe Basin and the Hudson Strait; referred to as HBS hereafter). In our sensitivity

simulations, we assess the potential contribution of this source region to DMS_g further north by estimating the DMS_{sw} based on primary productivity. We assumed that a) previously measured primary productivity values were representative of the year of our cruise and b) that the ratio of DMS_{sw} in Baffin Bay to DMS_{sw} in other bodies of water is the same as the ratio of primary productivity in Baffin Bay to primary productivity in other bodies of water. In effect, we assumed a linear relationship between DMS_{sw} and primary productivity. This assumption is in keeping with the (Simò and Dachs, 2002) parameterization for DMS_{sw}. We also note that Kameyama et al. (2013) use a related quantity, net community productivity, to parameterize DMS_{sw}, but net community productivity data was not available for the HBS. Ferland et al. (2011) found that the waters of Hudson Strait are as productive as those of the North Water (Northern Baffin Bay), while Hudson Bay and Foxe Basin are about a quarter as productive. Thus for our simulation we set the DMS_{sw} in Hudson Strait to be equal to that measured in the North Water, and the DMS_{sw} in Hudson Bay and Foxe Basin to a quarter of that value. In the absence of measurements, it is not possible to further constrain what the DMS_{sw} values might be in the Hudson Bay System.

2.3 Flux estimate calculations

Our 35 concurrent measurements of DMS in the atmosphere and seawater along the ship track in the Baffin Bay and Canadian Arctic Archipelago region allow us to estimate the air-sea flux of DMS. The flux is defined as the rate of transfer of a gas across a surface, in this case the surface of the ocean. For liquid-gas surfaces, the flux is described by Eq. 1,

$$F = -K_W \left(C_g/K_H - C_l\right) \tag{1}$$

where C_g and C_l are the concentrations of the chemical species of interest in the gas phase and liquid phase respectively, K_W is the transfer velocity, and K_H is the dimensionless gas over liquid form of the Henry's law constant (Johnson, 2010). The transfer velocity K_W is described by Eq. 2,

$$K_W = \left[\frac{1}{K_H k_a} + \frac{1}{k_w}\right]^{-1} \tag{2}$$

where K_W is composed of the single phase transfer velocities for both the water-side (k_w) and the air-side (k_a), representing the rates of transfer in each phase.

The transfer velocity for each phase encapsulates the physical processes controlling the flux in that phase. For soluble gases, the air-side processes play a more important role, and become increasingly relevant with increasing solubility, while insoluble gases exhibit exclusively water-side control (Wanninkhof et al., 2009). Air-sea fluxes are controlled by many different factors, which has led to the development of a proliferation of transfer velocity parameterizations, each addressing different issues. Some are physically based, i.e. attempt to mathematically describe the processes at play, while others are developed by fitting experimental or field data. It is not clear whether parameterizations developed based on measurements of the flux of a given gas can be applied to other gases. For

example, bubbles contribute less to the DMS flux than they do to the CO_2 flux, due to the limited solubility of carbon dioxide in water, and so parameterizations developed for CO_2 might be expected to overestimate the DMS flux (Blomquist et al., 2006). Indeed, recent studies have shown that the wind speed dependence of the DMS transfer velocity is close to linear (Huebert et al., 2010; Bell et al., 2013, 2015).

Fluxes were calculated according to Eq. 1 using the transfer velocity parameterizations of (Liss and Merlivat, 1986) and (Jeffery et al., 2010) for water-side and air-side, respectively (adjusted to the ambient seawater Schmidt number of DMS, details are in (Johnson, 2010)). Atmospheric concentrations were calculated from measured mixing ratios using measured atmospheric temperature, pressure, and the Henry's law constant for DMS at the in-situ temperature. Fluxes were multiplied by the fraction of open water in order to account for the capping effect of sea ice (Loose et al., 2014). The sea ice cover near the ship's location was estimated at a 0.5° x 0.5° resolution by plotting the ship's course at hourly resolution on daily ice charts obtained from the Canadian Ice Service (http://www.ec.gc.ca/glaces-ice/). These estimates were cross-referenced with daily photos taken aboard the ship to ensure accuracy. Estimates were made on a scale from 1-10, with no fractional values.

3 DMS mixing ratio observations and estimated fluxes

Figure 1b and Table 1 present the DMS_g mixing ratio data collected along the ship track. To our knowledge, these are the first DMS_g measurements for the Arctic during midsummer (July). These summertime measurements exceed previous measurements made in late summer and early fall by a factor of 3-10 (Table 1). This is consistent with the expectation of higher biological productivity in the summer than in other seasons (Levasseur, 2013). The time series exhibits high temporal variability. Three episodes of elevated DMS_g mixing ratios with values of 400 pptv or above occurred along the ship track on 18-20 July, 26 July and 1-2 August. Two episodes with DMS_g mixing ratios with values below 100 pptv occurred on 22-23 July and 5 August. Our values are on the same order (hundreds of pptv) as measurements made at high latitudes under bloom conditions in the Southern Ocean (Bell et al., 2015; Yang et al., 2011), the North Atlantic (Bell et al., 2013), and the North West Pacific (Tanimoto et al., 2013), but are higher than measurements made in the Tropical Pacific that were on the order of tens of pptv (Simpson et al., 2014).

Figure 2 presents the time series of DMS_g along the ship track together with both measured and GEOS wind speeds, DMS_{sw}, and our flux estimates. Previous DMS flux estimates for the Arctic are summarized in Table 2. The only other summertime estimate falls within the same range as in this work of ca. 0-10 μmol day^{-1}m^{-2} (Sharma et al., 1999b). A better constrained summer flux estimate for this region will require sampling of DMS_{sw} at higher spatial and temporal resolution,

and ideally direct continuous flux measurements using a technique such as eddy covariance, but these are challenging measurements rendered more so by the remoteness of Arctic Ocean.

4 Source sensitivity studies with GEOS-Chem and FLEXPART

In order to explore the provenance of the air masses being sampled on the ship, we used FLEXPART-WRF backward runs as well as GEOS-Chem simulations. Figure 3 summarizes our understanding of the origins of air masses arriving at the ship track. Figure 3A shows the time series of DMS_g from the GEOS-Chem simulation superimposed on the measured DMS_g time series, as well as the GEOS-Chem sea salt (a marine tracer) and methyl ethyl ketone and carbon monoxide (MEK and CO, biomass burning tracers) mixing ratios. Figure 3B shows the main land cover types in the region. Panel C in Fig. 3 shows examples of potential emissions sensitivity plots generated using FLEXPART-WRF that indicate regions the air has passed over before being sampled. Periods highlighted with a gray bar and numbered 1 through 3 were chosen as representative of three types of influence: 1) marine influence from south of the Arctic circle, 2) terrestrial influence from Northern Canada, and 3) regional marine influence from Baffin Bay. Sea salt tracer maxima indicate marine-influenced air and reflect high winds, while MEK and CO maxima indicate an influence from biomass burning. Biomass burning tracers provide a convenient indication of continental influence on the airmass. Figure 3 shows agreement between the sources of the air indicated by FLEXPART-WRF and by the GEOS-Chem tracers. For example, during Period 2 the MEK tracer is high and FLEXPART-WRF shows continental influence, while during Period 3 the sea salt tracer is high and FLEXPART-WRF shows marine influence.

4.1 Model-Measurement Comparison

In comparing the simulated DMS_g to our measurements, we assumed that the major cause of discrepancies between measurements and model was the representation of the DMS source in GEOS-Chem. Essentially, since the GEOS-Chem model has realistic capabilities in the simulation of transport (Kristiansen et al., 2016) and the chemical sinks of DMS are relatively well understood (Barnes et al., 2006), we chose to keep the transport and sink parameterizations constant for our sensitivity studies and focused on source sensitivity studies due to the considerable source-related uncertainty.

Figure 3a shows that our GEOS-Chem simulations reproduce the major features of the measured DMS_g time series, with appropriate magnitudes much of the time and an overall bias of -67 pptv. The poorest model-measurement agreements occur on 1-2 and 6-7 August, as shown in Fig. 4b and Fig. 3a, where GEOS-Chem overestimates DMS mixing ratios by a factor of 2-3. This overestimation coincides with high levels of the accumulation mode sea salt aerosol tracer in GEOS-Chem as shown in Fig. 3b. The overestimation may be due simulation errors related to the DMS_{sw} field, excessive GEOS wind speeds driving too large of a flux during this episode, or the performance of the air-sea

transfer velocity parameterization at high wind speeds. Wind speeds in our GEOS-Chem simulations display considerable scatter about the observed wind speeds along the ship track time series, but show a linear relationship with a slope of 0.95 and $R^2 = 0.35$ as in Fig. S4 and reproduce major features of the wind time series as in Fig. 2c. Overall, GEOS-Chem tended to overestimate DMS_g in Baffin Bay (largely open water at the time of the campaign) and underestimate it in Lancaster Sound (where we encountered between 10-100% ice cover). It is worth noting that the effect of sea ice on sea-air flux as hypothesized by Loose et al. (2014) is to increase the flux at low wind speeds and decrease it at high wind speeds. Implementation of this transfer velocity parameterization might be expected to improve model-measurement agreement. More work is needed to assess how best to parameterize air-sea flux in high latitude regions and the marginal ice zone in particular. Within these uncertainties, the seawater DMS source could largely account for the measured DMS_g. However, there are some notable mismatches that cannot be accounted for by the uncertainties detailed above. These are discussed in the following sections.

4.2 Seawater sources: Baffin Bay and Lancaster Sound as principal oceanic DMS source

Our model-measurement comparisons suggest that as expected, seawater makes the dominant contribution to the measured DMS_g. In this section, we examine the potential regional contributions. Figure 4a shows the relative contributions of various marine source regions to the GEOS-Chem simulation of the DMS_g along the ship track. Nearly 90% of the simulated DMS_g could be explained by the DMS oceanic emissions from Baffin Bay and Lancaster Sound when using the DMS_{sw} field based on our in situ measurements. The simulated DMS_g originating from Baffin Bay and Lancaster Sound are shown in blue and purple respectively in Fig.4a. These local emissions also contributed the majority of the highest mixing ratios observed during the campaign on 18 and 20 July. Overall, we conclude that the waters of Baffin Bay and Lancaster Sound acted as a strong local source of DMS_g throughout the campaign.

4.3 Transport from a seawater source: role of Hudson Bay System as an additional oceanic DMS source

Figure 4 shows that the simulated influence of the HBS is significant on 18-19 July, contributing up to 60% of simulated DMS_g towards the end of that time period. This peak in DMS coincided with a synoptic-scale storm system, which originated at lower latitudes and passed over Lancaster Sound, where the ship was located at the time. This transport pattern is visible in the FLEXPART-WRF retroplume for Period 1 in Fig. 3C. These results suggest that DMS emissions from the HBS are potentially an important source of atmospheric sulfur to the Arctic atmosphere during episodic transport events associated with mid latitude storms travelling northward. Our simulated results depend on the assumption that the DMS_{sw} values in the HBS are similar to those observed at higher latitudes. The potential for influence from the HBS is supported by previous reports of high levels

of DMS_g in air masses transported northward from the Hudson Bay region (Sjostedt et al., 2012). Measurements of both DMS_{sw} and DMS_g in the HBS are needed to confirm this hypothesis.

4.4 Investigation of possible missing sources

The GEOS-Chem simulated DMS_g time series underestimates the peaks in measured DMS_g on 17 and 26 July (shown in Fig. 3a). This mismatch coincides with a minimum in the simulated marine tracer (sea salt), suggesting that possibly a non-marine source of DMS_g is not being represented in the GEOS-Chem DMS parameterization. Since the emissions of DMS_g and sea salt aerosol are similarly dependent on wind speed and fraction of open ocean and their lifetimes are similarly short, we expect the DMS_g and sea salt tracers in our simulation to covary if the DMS_g is of marine origin. We note that the GEOS wind speeds are in good agreement with measured wind speeds during these time periods, as shown in Fig. 2c. It is possible that this model-measurement disagreement indicates that the model does not capture the true relationship of DMS_g to wind speed, or that the GEOS-Chem simulation is missing a coastal body of water at a sub-grid scale and that this water body was emitting large quantities of DMS. However, the FLEXPART-WRF retroplumes for 26 July (an example is shown as Period 2 of Fig. 3C) indicate that the airmass had spent most of its time over land surfaces and sea ice before reaching the ship's location. This continental air-mass origin is further supported by high levels of simulated continental tracers (e.g. MEK, shown in the third panel of Fig. 3a) during these same periods.

The suggestion that DMS_g may have a continental source is not new (Hopke et al., 1995), but has not received very much attention. The FLEXPART-WRF PES retroplumes indicate that the continental area influencing the air masses sampled by the ship was Northern Canada (primarily, regions to the south and east of Baffin Bay, including Nunavut and the Northwest Territories). The land cover in that region is shown in Fig. 3b and is a mixture of tundra, boreal forest, wetlands and lakes. As well, there was a wide spatial extent of melt ponds to the south and west of the ship track (shown in Fig. S5). To investigate the impact that each of these sources could have had on the DMS_g measured during the campaign, we estimated the DMS emission potential of each land cover type (including melt ponds) based on existing literature values. We implemented these extra emissions in the GEOS-Chem model and performed sensitivity tests to explore their potential to make additional contributions to DMS_g at the ship positions. These results are presented in the following subsections.

4.4.1 Emissions from melt ponds

Melt ponds form on the surface of sea ice as the snow melts. They cover much of the surface of the sea ice by mid summer and have been suggested as a potentially important source of DMS to the atmosphere (Levasseur, 2013). At the time of the campaign, the sea ice regions to the west and south of our ship track, particularly in Lancaster Sound, had considerable melt pond coverage as shown in Figure S5. The melt pond DMS source was implemented in GEOS-Chem by assuming that 50% of

sea ice was covered by melt ponds and treating melt ponds as seawater with a DMS_{sw} concentration of 3 nM (expected to be an upper limit based on Levasseur (2013). The Liss and Merlivat (1986) transfer velocity parameterization was used. The validity of assuming the same flux parameterization applies to a shallow melt pond as to the open ocean is untested, but is a reasonable approximation for our sensitivity test.

The blue curve in Fig. 4c shows the simulated DMS_g contribution for the melt pond source. The simulated melt pond contribution was greatest during 18-25 July when the ship was in Lancaster Sound. The maximum simulated melt pond contribution was about 100% on 23 July when simulated and measured DMS_g were very low. The strong contribution of the melt ponds at this time was likely due to the ship's position at the ice edge and advection of the arriving airmass over ice-covered regions. The simulated melt pond source contributed an average about 20% to the total simulated DMS_g over the remainder of the time series. Implementation of this source reduced the overall normalized mean model-measurement bias by 9%, suggesting that melt ponds could serve to elevate the regional background levels of DMS_g. Further measurements of DMS concentrations in melt ponds and, ideally, direct measurements of DMS fluxes from melt ponds are needed to better constrain the impact this source might have on DMS_g in the Arctic summer.

4.4.2 Emissions from coastal tundra

Previous studies suggest that DMS emissions from lichens (Gries et al., 1994) and from coastal tundra, particularly in regions where snow geese breed (Hines and Morrison, 1992), may be quite large. For lichens to emit reduced sulfur to the atmosphere, they require a source of sulfur. In coastal regions this can be supplied by sea spray. We implemented a tundra DMS source in GEOS-Chem by using the Olson Land Cover data (http://edc2.usgs.gov/glcc/globdoc2_0.php) to calculate the fraction of each GEOS-Chem grid box covered by the land type "barren tundra". We then assumed that 40% of that tundra (to account for inland regions emitting less due to less sulfate being deposited by sea spray) emitted DMS at a rate of 480 nM $m^{-2}h^{-1}$ (Hines and Morrison, 1992). We consider this simulation to give us an upper limit to the potential influence of tundra DMS emissions.

The results are presented as the brown curve in Fig. 4c. The simulated DMS_g at the ship track had the largest contribution from tundra sources during 16-17 July, with a maximum contribution to the simulated DMS_g at the ship position of 6%. The percent contribution was lower than that of the melt pond source because the tundra source acted to increase simulated DMS_g during times when levels were already high, but as can be seen in Fig. 4c the absolute contribution of the simulated tundra source was comparable to or greater than the melt pond source contribution. Like the melt pond source, the possible tundra source reduces the overall normalized mean bias (by 14%) and may contribute to the regional background levels of DMS_g. However, neither source can account for the large unexplained peaks in the measured time series.

4.4.3 Emissions from lakes

To evaluate the potential contribution of DMS from lakes, the fresh water fraction in each GEOS-Chem grid box in a rectangular domain spanning 48 to 75°N and -68 to -140°W was calculated using the Olson Land Cover map, at 1 km x 1 km resolution. Based on the work of Sharma et al. (1999a), we assigned a mean value of 1 nM DMS to the fresh water in that domain. We then applied the same Liss and Merlivat (1986) parameterization to the fraction of the grid box with lake coverage. The same caveats apply to the use of transfer velocity parameterizations developed for the open ocean for fluxes from lakes as to the application to melt ponds as discussed above. In our simulation, the lake source was only locally important as shown in Fig. 5. There was a modest contribution to the absolute magnitude of DMS_g in Northern Quebec and Labrador, and had negligible effects elsewhere. The percent change in surface layer DMS_g in the Northwest Territories was quite large due to there being no other simulated sources of DMS_g in that location, but the absolute values of DMS_g are very small. However, as there are few measurements of DMS concentrations in lakes in Northern Canada, we cannot exclude the possibility that the actual lake concentrations of DMS_{sw} are much higher than 1 nM and that the unexplained peak in our time series is due to a lake source of DMS_g. This possibility is supported by high chlorophyll-α levels in the lakes of Northern Canada (shown in Fig. S6) and the fact that the measurements of DMS_{sw} in lakes that we used for this sensitivity test were made more than 15 years ago, and the high northern latitudes have warmed significantly since then (IPCC, 2013).

4.4.4 Other potential DMS sources for the study area

Due to the paucity of measurements of DMS emissions from vegetation, boreal soils, and Arctic wetlands, especially during and in proximity to biomass burning events, this potential missing source is very difficult to evaluate. The correlation between the measurement-model residual and the biomass burning tracers in GEOS-Chem shown in Fig. 3A suggests that DMS_g was being co-transported with these biomass burning tracers. The measurement-model difference and the MEK tracer have a similar peak on 26 July as shown in Fig. 3A. The FLEXPART-WRF retroplumes (e.g. Period 2 in Fig. 3) identify this time as being continentally influenced.

DMS emissions have been reported from biomass burning (Akagi et al., 2011; Meinardi et al., 2003). Summer 2014 was a particularly active wildfire season in Northern Canada (Blunden and Arndt, 2015). The simplest reason for the maxima in biomass burning tracers during the unexplained DMS_g peak on 26 July would be emissions of DMS from biomass burning that are not represented in the model. To gauge the importance of this source to DMS_g in the Arctic, we used the emission factor for DMS from boreal forest biomass burning reported by Akagi et al. (2011). We indexed the simulated DMS emissions to CO emissions, such that 3.66×10^{-5} molecules of DMS are emitted for each molecule of CO emitted. Figure 5 shows that the biomass burning sensitivity test indicated

that the biomass burning source of DMS_g had local influence only, like the modelled lake source. The reason for this is that the emission factor for DMS from boreal forest fires is not very large. As a result, this source acted to increase DMS_g in the immediate vicinity of the wildfires in the Northwest Territories, but had a negligible influence on the time series and is therefore not shown in Fig. 4. The biomass burning source of DMS_g was likely not sufficient to directly influence the DMS_g time series at the ship position, unless the emission factor used in the model is an order of magnitude too low. This seems unlikely as the emission factor we used was derived from direct measurements in a biomass burning plume originating from the boreal forest (Akagi et al., 2011). Considerably larger DMS emissions have been measured from other types of biomass burning in other locations (Meinardi et al., 2003) but we have no measurement evidence to support a higher emissions factor in our present simulations. We note that in particular, emissions from tundra fires are completely unconstrained and might be quite different from emissions from boreal forest fires due to different vegetation types and different types of burning (e.g. open flames versus smoldering). Further study is required.

Although the available information suggests that direct DMS emissions from fires seem unlikely to explain the bias, support for the hypothesis that DMS_g is being co-transported with biomass burning tracers is given by improved model-measurement agreement indicated by Fig. 3c if we assume the biomass burning plume contains equal amounts of DMS_g and MEK, and add this DMS_g "source" to the simulated DMS_g. This revision reduces the overall measurement-model bias by 24 %, and reduces the residual by 200 pptv for the 26 July. Alternatively, the air mass observed at the ship could have passed over a strong near-land marine source, which is missing in our simulations. However, the FLEXPART-WRF simulation indicates that the air-mass had travelled over nearly entirely ice-covered regions before arriving at the ship, suggesting that a marine source is a less likely explanation for the observed DMS_g.

Emissions of reduced sulfur species from both soils and lakes are temperature dependent (Bates et al., 1992), suggesting that the wild fires could indirectly promote DMS emissions. Proximity to wild fires could increase the temperature of the soil as well as changing the air quality, which might stress biota. A mechanism whereby biomass burning increases the emission of reduced sulfur species such as DMS from soils, lakes and vegetation might yield increased emissions but this requires further study and we do not have any information that would allow implementation of this possible effect in our simulations.

5 Conclusions

This study presents, to the best of our knowledge, the first measurements of gaseous DMS mixing ratios in the summertime Arctic atmosphere of Baffin Bay and parts of the Canadian Arctic Archipelago. Measured DMS_g values were greater than those measured in fall in the same region

(consistent with higher biological productivity in summer) and broadly consistent with measurements in other parts of the ocean. We made flux estimates that fall within the range of existing DMS air-sea flux estimates for the summertime Central Arctic Ocean. The data presented here improve our knowledge of atmospheric DMS levels in the summertime Arctic, but further study is needed to understand spatial, seasonal and interannual variability of DMS both in the ocean and in the atmosphere.

We conducted sensitivity simulations with the GEOS-Chem chemical transport model to examine the potential of various sources to contribute to DMS_g measured along the ship track. We found that local oceanic sources can account for a large proportion (70% overall) of the atmospheric surface-layer DMS measured along our ship track in the Canadian Arctic Archipelago and Baffin Bay during summer 2014. Our GEOS-Chem simulations indicated that during transport events associated with synoptic-scale storms, marine sources south of the Arctic Circle made strong and episodic contributions (as much as 60%) to DMS mixing ratios in the Canadian Arctic Archipelago region. The role of transport in controlling DMS levels and the potential for aerosol particle formation from DMS_g has been argued convincingly in a global sense by Quinn and Bates (2011). We propose that it may also be important episodically in the Arctic, e.g. transport from the Hudson Bay System or the Northwest Territories. These origins for air at our ship track are also supported by FLEXPART-WRF retroplume analysis.

GEOS-Chem simulations were biased low by 67 pptv over the ship track time series (representing between 10% to 100% of the measured mixing ratios). We investigated several additional sources (tundra, forests, lakes and melt ponds), which could contribute to surface layer DMS mixing ratios. Our sensitivity simulations indicated maximum contributions of 6% and 100% from tundra and melt ponds, respectively, to the simulated total DMS_g for the ship-track time series, suggesting that emissions of DMS from melt ponds and coastal tundra could have important local, regional effects on DMS levels. These sensitivity studies also suggest that terrestrial or near-terrestrial sources could make additional contributions to DMS_g in our study region. These emissions may be related to changes in lake, forest and soil emissions due to the heat and stress associated with biomass burning. Flux measurements from melt ponds and the boreal forest and lakes, particularly when under stress from biomass burning events, are needed to evaluate this hypothesis.

Our findings have implications for our understanding of the sulfur cycle in the summer Arctic and how it has changed in the recent past and will continue to change in the future. For example, much of the discussion surrounding changes in Arctic DMS has focused on the loss of sea ice (Levasseur, 2013), but the loss of permafrost might also have a large impact through changing nutrient levels in lakes (Rhüland and Smol, 1998). The potential influence of the observed atmospheric levels of DMS on new particle formation and subsequent growth remains to be explored.

Author contributions

J. Abbatt and M. Levasseur designed the experiments and E. Mungall and M. Lizotte carried them out. J. Murphy, J. Liggio and J. Wentzell facilitated the *Amundsen* campaign. B. Croft and J. Thomas performed the GEOS-Chem and FLEXPART-WRF simulations, respectively. E. Mungall carried out the analysis, and E. Mungall prepared the manuscript with the aid of B. Croft and contributions from all co-authors.

Acknowledgements. The authors would like to acknowledge the financial support of NSERC for the NETCARE project funded under the Climate Change and Atmospheric Research program. As well, we thank ArcticNet for hosting NETCARE scientists on the *Amundsen*, in particular the help of Keith Levesque, and all of the crew and scientists aboard. Additionally, special thanks to Amir Aliabadi, Ralf Staebler, Lauren Candlish, Heather Stark, Tonya Burgers and Tim Papakyriakou for ozone sondes and meteorological data. Thanks to Michelle Kim and Tim Bertram of UCSD for invaluable discussions of ion chemistry. The authors thank K. Tavis and P. Kim for their assistance in implementation of the QFED2 database.

References

Akagi, S. K., Yokelson, R. J., Wiedinmyer, C., Alvarado, M. J., Reid, J. S., Karl, T., Crounse, J. D., and Wennberg, P. O.: Emission factors for open and domestic biomass burning for use in atmospheric models, Atmos. Chem. Phys., 11, 4039–4072, doi:10.5194/acp-11-4039-2011, 2011.

Albrecht, B. A.: Aerosols, cloud microphysics, and fractional cloudiness, Science, 245, 1227–1230, 1989.

Alexander, B., Park, R. J., Jacob, D. J., Li, Q., Yantosca, R. M., Savarino, J., Lee, C., and Thiemens, M.: Sulfate formation in sea-salt aerosols: Constraints from oxygen isotopes, J. Geophys. Res.-Atmos., 110, 2005.

Alexander, B., Park, R. J., Jacob, D. J., and Gong, S.: Transition metal-catalyzed oxidation of atmospheric sulfur: Global implications for the sulfur budget, J. Geophys. Res.-Atmos., 114, 2009.

Allgood, C., Lin, Y., Ma, Y.-C., and Munson, B.: Benzene as a selective chemical ionization reagent gas, Org. Mass Spectrom., 25, 497–502, doi:10.1002/oms.1210251003, 1990.

Barnes, I., Hjorth, J., and Mihalopoulos, N.: Dimethyl Sulfide and Dimethyl Sulfoxide and Their Oxidation in the Atmosphere, Chem. Rev., 106, 940–975, doi:10.1021/cr020529+, 2006.

Bates, T. S., Lamb, B. K., Guenther, A., Dignon, J., and Stoiber, R. E.: Sulfur emissions to the atmosphere from natural sourees, J. Atmos. Chem., 14, 315–337, doi:10.1007/BF00115242, 1992.

Bell, T. G., De Bruyn, W., Miller, S. D., Ward, B., Christensen, K. H., and Saltzman, E. S.: Air–sea dimethylsulfide (DMS) gas transfer in the North Atlantic: evidence for limited interfacial gas exchange at high wind speed, Atmos. Chem. Phys., 13, 11 073–11 087, doi:10.5194/acp-13-11073-2013, 2013.

Bell, T. G., De Bruyn, W., Marandino, C. A., Miller, S. D., Law, C. S., Smith, M. J., and Saltzman, E. S.: Dimethylsulfide gas transfer coefficients from algal blooms in the Southern Ocean, Atmos. Chem. Phys., 15, 1783–1794, doi:10.5194/acp-15-1783-2015, 2015.

Bey, I., Jacob, D. J., Yantosca, R. M., Logan, J. A., Field, B. D., Fiore, A. M., Li, Q., Liu, H. Y., Mickley, L. J., and Schultz, M. G.: Global modeling of tropospheric chemistry with assimilated meteorology: Model description and evaluation, 2001.

Blomquist, B. W., Fairall, C. W., Huebert, B. J., Kieber, D. J., and Westby, G. R.: DMS sea-air transfer velocity: Direct measurements by eddy covariance and parameterization based on the NOAA/COARE gas transfer model, Geophys. Res. Lett., 33, doi:10.1029/2006GL025735, 2006.

Blunden, J. and Arndt, D. S.: State of the Climate in 2014, B. Am. Meteorol. Soc., 96, ES1–ES32, doi:10.1175/2015BAMSStateoftheClimate.1, 2015.

Breider, T. J., Mickley, L. J., Jacob, D. J., Wang, Q., Fisher, J. A., Chang, R. Y.-W., and Alexander, B.: Annual distributions and sources of Arctic aerosol components, aerosol optical depth, and aerosol absorption, J. Geophys. Res-Atmos., 119, 4107–4124, doi:10.1002/2013JD020996, 2014.

Brioude, J., Arnold, D., Stohl, A., Cassiani, M., Morton, D., Seibert, P., Angevine, W., Evan, S., Dingwell, A., Fast, J. D., Easter, R. C., Pisso, I., Burkhart, J., and Wotawa, G.: The Lagrangian particle dispersion model FLEXPART-WRF version 3.1, Geosci. Model Dev., 6, 1889–1904, doi:10.5194/gmd-6-1889-2013, 2013.

Browse, J., Carslaw, K. S., Arnold, S. R., Pringle, K., and Boucher, O.: The scavenging processes controlling the seasonal cycle in Arctic sulphate and black carbon aerosol, Atmos. Chem. Phys., 12, 6775–6798, doi:10.5194/acp-12-6775-2012, 2012.

Carslaw, K. S., Lee, L. A., Reddington, C. L., Pringle, K. J., Rap, A., Forster, P. M., Mann, G. W., Spracklen, D. V., Woodhouse, M. T., Regayre, L. A., and Pierce, J. R.: Large contribution of natural aerosols to uncertainty in indirect forcing, Nature, 503, 67–71, doi:10.1038/nature12674, 2013.

Chang, R. Y.-W., Sjostedt, S. J., Pierce, J. R., Papakyriakou, T. N., Scarratt, M. G., Michaud, S., Levasseur, M., Leaitch, W. R., and Abbatt, J. P. D.: Relating atmospheric and oceanic DMS levels to particle nucleation events in the Canadian Arctic, J. Geophys. Res.-Atmos., 116, D00S03, doi:10.1029/2011JD015926, 2011.

Charlson, R. J., Lovelock, J. E., Andreae, M. O., and Warren, S. G.: Oceanic phytoplankton, atmospheric sulphur, cloud albedo and climate, Nature, 326, 655–661, doi:10.1038/326655a0, 1987.

Chen, H., Ezell, M. J., Arquero, K. D., Varner, M. E., Dawson, M. L., Gerber, R. B., and Finlayson-Pitts, B. J.: New particle formation and growth from methanesulfonic acid, trimethylamine and water, Phys. Chem. Chem. Phys., doi:10.1039/C5CP00838G, 2015.

Croft, B., Martin, R. V., Leaitch, W. R., Tunved, P., Breider, T. J., D'Andrea, S. D., and Pierce, J. R.: Processes controlling the annual cycle of Arctic aerosol number and size distributions, Atmos. Chem. Phys., 16, 3665–3682, doi:10.5194/acp-16-3665-2016, 2016.

Darmenov, A. and da Silva, A.: The quick fire emissions dataset (QFED)–documentation of versions 2.1, 2.2 and 2.4, NASA Technical Report Series on Global Modeling and Data Assimilation, NASA TM-2013-104606, 32, 183, 2013.

Erickson, D. J., Ghan, S. J., and Penner, J. E.: Global ocean-to-atmosphere dimethyl sulfide flux, J. Geophys. Res.-Atmos., 95, 7543–7552, doi:10.1029/JD095iD06p07543, 1990.

Fairlie, T. D., Jacob, D. J., and Park, R. J.: The impact of transpacific transport of mineral dust in the United States, Atmos. Environ., 41, 1251–1266, 2007.

Fairlie, T. D., Jacob, D. J., Dibb, J. E., Alexander, B., Avery, M. A., Donkelaar, A. v., and Zhang, L.: Impact of mineral dust on nitrate, sulfate, and ozone in transpacific Asian pollution plumes, Atmos. Chem. Phys., 10, 3999–4012, 2010.

Ferland, J., Gosselin, M., and Starr, M.: Environmental control of summer primary production in the Hudson Bay system: The role of stratification, J. Marine Syst., 88, 385–400, doi:10.1016/j.jmarsys.2011.03.015, 2011.

Fisher, J. A., Jacob, D. J., Wang, Q., Bahreini, R., Carouge, C. C., Cubison, M. J., Dibb, J. E., Diehl, T., Jimenez, J. L., Leibensperger, E. M., et al.: Sources, distribution, and acidity of sulfate–ammonium aerosol in the Arctic in winter–spring, Atmos. Environ., 45, 7301–7318, 2011.

Fisher, J. A., Jacob, D. J., Soerensen, A. L., Amos, H. M., Steffen, A., and Sunderland, E. M.: Riverine source of Arctic Ocean mercury inferred from atmospheric observations, Nat. Geosci., 5, 499–504, 2012.

Fountoukis, C. and Nenes, A.: ISORROPIA II: a computationally efficient thermodynamic equilibrium model for K+–Ca 2+–Mg 2+–NH 4+–Na+–SO 4 2—NO 3—Cl—H 2 O aerosols, Atmos. Chem. Phys., 7, 4639–4659, 2007.

Gries, C., Iii, T. H. N., and Kesselmeier, J.: Exchange of reduced sulfur gases between lichens and the atmosphere, Biogeochemistry, 26, 25–39, doi:10.1007/BF02180402, 1994.

Hines, M. E. and Morrison, M. C.: Emissions of biogenic sulfur gases from Alaskan tundra, J. Geophys. Res.-Atmos., 97, 16 703–16 707, doi:10.1029/90JD02576, 1992.

Hopke, P. K., Barrie, L. A., Li, S.-M., Cheng, M.-D., Li, C., and Xie, Y.: Possible sources and preferred pathways for biogenic and non-sea-salt sulfur for the high Arctic, J. Geophys. Res.-Atmos., 100, 16 595–16 603, doi:10.1029/95JD01712, 1995.

Huebert, B. J., Blomquist, B. W., Yang, M. X., Archer, S. D., Nightingale, P. D., Yelland, M. J., Stephens, J., Pascal, R. W., and Moat, B. I.: Linearity of DMS transfer coefficient with both friction velocity and wind speed in the moderate wind speed range, Geophys. Res. Lett., 37, L01 605, doi:10.1029/2009GL041203, 2010.

IPCC: Summary for Policymakers, in: Climate Change 2013: The Physical Science Basis. Contribution of Working Group I to the Fifth Assessment Report of the Intergovernmental Panel on Climate Change, edited by Stocker, T., Qin, D., Plattner, G.-K., Tignor, M., Allen, S., Boschung, J., Nauels, A., Xia, Y., Bex, V., and Midgley, P., pp. 1–30, Cambridge University Press, Cambridge, United Kingdom and New York, NY, USA, 2013.

Jardine, K., Abrell, L., Kurc, S. A., Huxman, T., Ortega, J., and Guenther, A.: Volatile organic compound emissions from Larrea tridentata (creosotebush), Atmos. Chem. Phys., 10, 12 191–12 206, doi:10.5194/acp-10-12191-2010, 2010.

Jardine, K., Yañez-Serrano, A., Williams, J., Kunert, N., Jardine, A., Taylor, T., Abrell, L., Artaxo, P., Guenther, A., Hewitt, C., House, E., Florentino, A. P., Manzi, A., Higuchi, N., Kesselmeier, J., Behrendt, T., Veres, P. R., Derstroff, B., Fuentes, J. D., Martin, S., and Andreae, M. O.: Dimethyl Sulfide in the Amazon Rain Forest, Global Biogeochem. Cy., p. 2014GB004969, doi:10.1002/2014GB004969, 2014.

Jeffery, C. D., Robinson, I. S., and Woolf, D. K.: Tuning a physically-based model of the air–sea gas transfer velocity, Ocean Model., 31, 28–35, doi:10.1016/j.ocemod.2009.09.001, 2010.

Jodwalis, C. M., Benner, R. L., and Eslinger, D. L.: Modeling of dimethyl sulfide ocean mixing, biological production, and sea-to-air flux for high latitudes, J. Geophys. Res.-Atmos., 105, 14 387–14 399, doi:10.1029/2000JD900023, 2000.

Johnson, M. T.: A numerical scheme to calculate temperature and salinity dependent air-water transfer velocities for any gas, Ocean Sci., 6, 913–932, doi:10.5194/os-6-913-2010, 2010.

Kameyama, S., Tanimoto, H., Inomata, S., Yoshikawa-Inoue, H., Tsunogai, U., Tsuda, A., Uematsu, M., Ishii, M., Sasano, D., Suzuki, K., and Nosaka, Y.: Strong relationship between dimethyl sulfide and net community production in the western subarctic Pacific, Geophysical Research Letters, 40, 3986–3990, doi:10.1002/grl.50654, 2013.

Kim, M. J., Zoerb, M. C., Campbell, N. R., Zimmermann, K. J., Blomquist, B. W., Huebert, B. J., and Bertram, T. H.: Revisiting benzene cluster cations for the chemical ionization of dimethyl sulfide and select volatile organic compounds, Atmos. Meas. Tech. Discuss., 8, 10 121–10 157, doi:10.5194/amtd-8-10121-2015, 2015.

K ohler, H.: The nucleus in and the growth of hygroscopic droplets, Transactions of the Faraday Society, 32, 1152–1161, doi:10.1039/TF9363201152, 1936.

Kristiansen, N. I., Stohl, A., Olivié, D. J. L., Croft, B., Søvde, O. A., Klein, H., Christoudias, T., Kunkel, D., Leadbetter, S. J., Lee, Y. H., Zhang, K., Tsigaridis, K., Bergman, T., Evangeliou, N., Wang, H., Ma, P.-L., Easter, R. C., Rasch, P. J., Liu, X., Pitari, G., Di Genova, G., Zhao, S. Y., Balkanski, Y., Bauer, S. E., Faluvegi, G. S., Kokkola, H., Martin, R. V., Pierce, J. R., Schulz, M., Shindell, D., Tost, H., and Zhang, H.: Evaluation

of observed and modelled aerosol lifetimes using radioactive tracers of opportunity and an ensemble of 19 global models, Atmos. Chem. Phys., 16, 3525–3561, doi:10.5194/acp-16-3525-2016, 2016.

Lana, A., Bell, T. G., Simó, R., Vallina, S. M., Ballabrera-Poy, J., Kettle, A. J., Dachs, J., Bopp, L., Saltzman, E. S., Stefels, J., Johnson, J. E., and Liss, P. S.: An updated climatology of surface dimethlysulfide concentrations and emission fluxes in the global ocean, Global Biogeochem. Cy., 25, GB1004, doi:10.1029/2010GB003850, 2011.

Leaitch, W. R., Sharma, S., Huang, L., Toom-Sauntry, D., Chivulescu, A., Macdonald, A. M., von Salzen, K., Pierce, J. R., Bertram, A. K., Schroder, J. C., Shantz, N. C., Chang, R. Y.-W., and Norman, A.-L.: Dimethyl sulfide control of the clean summertime Arctic aerosol and cloud, Elementa, 1, 000 017, doi:10.12952/journal.elementa.000017, 2013.

Leck, C. and Persson, C.: The central Arctic Ocean as a source of dimethyl sulfide Seasonal variability in relation to biological activity, Tellus B, 48, 156–177, doi:10.1034/j.1600-0889.1996.t01-1-00003.x, 1996.

Levasseur, M.: Impact of Arctic meltdown on the microbial cycling of sulphur, Nature Geosci., 6, 691–700, doi:10.1038/ngeo1910, 2013.

Liao, H., Henze, D. K., Seinfeld, J. H., Wu, S., and Mickley, L. J.: Biogenic secondary organic aerosol over the United States: Comparison of climatological simulations with observations, J. Geophys. Res.-Atmos., 112, 2007.

Liss, P. S. and Merlivat, L.: Air-sea gas exchange rates: Introduction and synthesis, in: The role of air-sea exchange in geochemical cycling, pp. 113–127, Springer, 1986.

Lizotte, M., Levasseur, M., Michaud, S., Scarratt, M. G., Merzouk, A., Gosselin, M., Pommier, J., Rivkin, R. B., and Kiene, R. P.: Macroscale patterns of the biological cycling of dimethylsulfoniopropionate (DMSP) and dimethylsulfide (DMS) in the Northwest Atlantic, Biogeochem., 110, 183–200, doi:10.1007/s10533-011-9698-4, 2012.

Loose, B., McGillis, W. R., Perovich, D., Zappa, C. J., and Schlosser, P.: A parameter model of gas exchange for the seasonal sea ice zone, Ocean Sci., 10, 17–28, doi:10.5194/os-10-17-2014, 2014.

Macdonald, R. W., Kuzyk, Z. A., and Johannessen, S. C.: It is not just about the ice: a geochemical perspective on the changing Arctic Ocean, J. Environ. Sci., pp. 1–14, doi:10.1007/s13412-015-0302-4, 2015.

Mauritsen, T., Sedlar, J., Tjernström, M., Leck, C., Martin, M., Shupe, M., Sjogren, S., Sierau, B., Persson, P. O. G., Brooks, I. M., and Swietlicki, E.: An Arctic CCN-limited cloud-aerosol regime, Atmos. Chem. Phys., 11, 165–173, doi:10.5194/acp-11-165-2011, 2011.

Meinardi, S., Simpson, I. J., Blake, N. J., Blake, D. R., and Rowland, F. S.: Dimethyl disulfide (DMDS) and dimethyl sulfide (DMS) emissions from biomass burning in Australia, Geophys. Res. Lett., 30, 1454, doi:10.1029/2003GL016967, 2003.

Nilsson, E. D. and Leck, C.: A pseudo-Lagrangian study of the sulfur budget in the remote Arctic marine boundary layer, Tellus B, 54, 213–230, doi:10.1034/j.1600-0889.2002.01247.x, 2002.

Nriagu, J. O., Holdway, D. A., and Coker, R. D.: Biogenic Sulfur and the Acidity of Rainfall in Remote Areas of Canada, Science, 237, 1189–1192, doi:10.1126/science.237.4819.1189, 1987.

Park, R. J., Jacob, D. J., Chin, M., and Martin, R. V.: Sources of carbonaceous aerosols over the United States and implications for natural visibility, J. Geophys. Res.-Atmos., 108, 2003.

Park, R. J., Jacob, D. J., Field, B. D., Yantosca, R. M., and Chin, M.: Natural and transboundary pollution influences on sulfate-nitrate-ammonium aerosols in the United States: Implications for policy, J. Geophys. Res.-Atmos., 109, 2004.

Park, R. J., Jacob, D. J., Kumar, N., and Yantosca, R. M.: Regional visibility statistics in the United States: Natural and transboundary pollution influences, and implications for the Regional Haze Rule, Atmos. Environ., 40, 5405–5423, 2006.

Patris, N., Delmas, R., Legrand, M., De Angelis, M., Ferron, F. A., Stiévenard, M., and Jouzel, J.: First sulfur isotope measurements in central Greenland ice cores along the preindustrial and industrial periods, J. Geophys. Res.-Atmos., 107, ACH 6–1, doi:10.1029/2001JD000672, 2002.

Pirjola, L., Kulmala, M., Wilck, M., Bischoff, A., Stratmann, F., and Otto, E.: Formation of sulphuric acid aerosols and cloud condensation nuclei: an expression for significant nucleation and model comparison, J. Aerosol Sci., 30, 1079–1094, doi:10.1016/S0021-8502(98)00776-9, 1999.

Quinn, P. K. and Bates, T. S.: The case against climate regulation via oceanic phytoplankton sulphur emissions, Nature, 480, 51–56, doi:10.1038/nature10580, 2011.

Rempillo, O., Seguin, A. M., Norman, A.-L., Scarratt, M., Michaud, S., Chang, R., Sjostedt, S., Abbatt, J., Else, B., Papakyriakou, T., Sharma, S., Grasby, S., and Levasseur, M.: Dimethyl sulfide air-sea fluxes and biogenic sulfur as a source of new aerosols in the Arctic fall, J. Geophys. Res.-Atmos., 116, D00S04, doi:10.1029/2011JD016336, 2011.

Rhüland, K. and Smol, J. P.: Limnological Characteristics of 70 Lakes Spanning Arctic Treeline from Coronation Gulf to Great Slave Lake in the Central Northwest Territories, Canada, Int. Rev. Hydrobiol., 83, 183–203, doi:10.1002/iroh.19980830302, 1998.

Richards, S. R., Rudd, J. W. M., and Kelly, C. A.: Organic volatile sulfur in lakes ranging in sulfate and dissolved salt concentration over five orders of magnitude, Limnol. Oceanogr., 39, 562–572, doi:10.4319/lo.1994.39.3.0562, 1994.

Rosel, A. and Kaleschke, L.: Exceptional melt pond occurrence in the years 2007 and 2011 on the Arctic sea ice revealed from MODIS satellite data, J. Geophys. Res.-Oceans, 117, C05 018, doi:10.1029/2011JC007869, 2012.

Scarratt, M. G., Levasseur, M., Schultes, S., Michaud, S., Cantin, G., Vezina, A., Gosselin, M., and De Mora, S. J.: Production and consumption of dimethylsulfide (DMS) in North Atlantic waters, Mar. Ecol. Prog. Ser., 204, 13–26, 2000.

Sharma, S., Barrie, L. A., Hastie, D. R., and Kelly, C.: Dimethyl sulfide emissions to the atmosphere from lakes of the Canadian boreal region, J. Geophys. Res.-Atmos., 104, 11 585–11 592, doi:10.1029/1999JD900127, 1999a.

Sharma, S., Barrie, L. A., Plummer, D., McConnell, J. C., Brickell, P. C., Levasseur, M., Gosselin, M., and Bates, T. S.: Flux estimation of oceanic dimethyl sulfide around North America, J. Geophys. Res.-Atmos., 104, 21 327–21 342, doi:10.1029/1999JD900207, 1999b.

Sharma, S., Chan, E., Ishizawa, M., Toom-Sauntry, D., Gong, S. L., Li, S. M., Tarasick, D. W., Leaitch, W. R., Norman, A., Quinn, P. K., Bates, T. S., Levasseur, M., Barrie, L. A., and Maenhaut, W.: Influence of transport and ocean ice extent on biogenic aerosol sulfur in the Arctic atmosphere, J. Geophys. Res.-Atmos., 117, D12 209, doi:10.1029/2011JD017074, 2012.

Simò, R. and Dachs, J.: Global ocean emission of dimethylsulfide predicted from biogeophysical data, Global Biogeochemical Cycles, 16, 1078, doi:10.1029/2001GB001829, 2002.

Simpson, R. M. C., Howell, S. G., Blomquist, B. W., Clarke, A. D., and Huebert, B. J.: Dimethyl sulfide: Less important than long-range transport as a source of sulfate to the remote tropical Pacific marine boundary layer, J. Geophys. Res.-Atmos., 119, 9142–9167, doi:10.1002/2014JD021643, 2014.

Sjostedt, S. J., Leaitch, W. R., Levasseur, M., Scarratt, M., Michaud, S., Motard-Côté, J., Burkhart, J. H., and Abbatt, J. P. D.: Evidence for the uptake of atmospheric acetone and methanol by the Arctic Ocean during late summer DMS-Emission plumes, J. Geophys. Res.-Atmos., 117, n/a–n/a, doi:10.1029/2011JD017086, 2012.

Skamarock, W. C., Klemp, J. B., Dudhia, J., Gill, D. O., Barker, D. M., Wang, W., and Powers, J. G.: A description of the advanced research WRF version 2, Tech. rep., DTIC Document, 2005.

Smith, S. R., Bourassa, M. A., and Sharp, R. J.: Establishing more truth in true winds, J. Atmos. Oceanic Technol., 16, 939–952, 1999.

Stohl, A., Forster, C., Frank, A., Seibert, P., and Wotawa, G.: Technical note: The Lagrangian particle dispersion model FLEXPART version 6.2, Atmos. Chem. Phys., 5, 2461–2474, doi:10.5194/acp-5-2461-2005, 2005.

Tanimoto, H., Kameyama, S., Iwata, T., Inomata, S., and Omori, Y.: Measurement of Air-Sea Exchange of Dimethyl Sulfide and Acetone by PTR-MS Coupled with Gradient Flux Technique, Environ. Sci. Tech., doi:10.1021/es4032562, 2013.

Tesdal, J.-E., Christian, J., Monahan, A., and von Salzen, K.: Sensitivity of modelled sulfate radiative forcing to DMS concentration and air-sea flux formulation, Atmos. Chem. Phys. Discuss., 15, 23 931–23 968, 2015.

Tilling, R. L., Ridout, A., Shepherd, A., and Wingham, D. J.: Increased Arctic sea ice volume after anomalously low melting in 2013, Nat. Geosci., advance online publication, doi:10.1038/ngeo2489, 2015.

Tjernström, M., Leck, C., Birch, C. E., Bottenheim, J. W., Brooks, B. J., Brooks, I. M., Bäcklin, L., Chang, R. Y.-W., de Leeuw, G., Di Liberto, L., de la Rosa, S., Granath, E., Graus, M., Hansel, A., Heintzenberg, J., Held, A., Hind, A., Johnston, P., Knulst, J., Martin, M., Matrai, P. A., Mauritsen, T., Müller, M., Norris, S. J., Orellana, M. V., Orsini, D. A., Paatero, J., Persson, P. O. G., Gao, Q., Rauschenberg, C., Ristovski, Z., Sedlar, J., Shupe, M. D., Sierau, B., Sirevaag, A., Sjogren, S., Stetzer, O., Swietlicki, E., Szczodrak, M., Vaattovaara, P., Wahlberg, N., Westberg, M., and Wheeler, C. R.: The Arctic Summer Cloud Ocean Study (ASCOS): overview and experimental design, Atmos. Chem. Phys., 14, 2823–2869, doi:10.5194/acp-14-2823-2014, 2014.

Twomey, S.: The Influence of Pollution on the Shortwave Albedo of Clouds, J. Atmos. Sci., 34, 1149–1152, doi:10.1175/1520-0469(1977)034<1149:TIOPOT>2.0.CO;2, 1977.

Wang, Q., Jacob, D. J., Fisher, J. A., Mao, J., Leibensperger, E. M., Carouge, C. C., Le Sager, P., Kondo, Y., Jimenez, J. L., Cubison, M. J., and Doherty, S. J.: Sources of carbonaceous aerosols and deposited black carbon in the Arctic in winter-spring: implications for radiative forcing, Atmos. Chem. Phys., 11, 12 453–12 473, doi:10.5194/acp-11-12453-2011, 2011.

Wanninkhof, R., Asher, W. E., Ho, D. T., Sweeney, C., and McGillis, W. R.: Advances in Quantifying Air-Sea Gas Exchange and Environmental Forcing*, Annu. Rev. Mar. Sci., 1, 213–244, doi:10.1146/annurev.marine.010908.163742, 2009.

Watts, S. F.: The mass budgets of carbonyl sulfide, dimethyl sulfide, carbon disulfide and hydrogen sulfide, Atmos. Environ., 34, 761–779, doi:10.1016/S1352-2310(99)00342-8, 2000.

Wentworth, G. R., Murphy, J. G., Croft, B., Martin, R. V., Pierce, J. R., Ct.-S., Courchesne, I., Tremblay, J.-., Gagnon, J., Thomas, J. L., Sharma, S., Toom-Sauntry, D., Chivulescu, A., Levasseur, M., and Abbatt, J. P. D.: Ammonia in the summertime Arctic marine boundary layer: sources, sinks, and implications, Atmos. Chem. Phys., 16, 1937–1953, doi:10.5194/acp-16-1937-2016, 2016.

Yang, M., Blomquist, B. W., Fairall, C. W., Archer, S. D., and Huebert, B. J.: Air-sea exchange of dimethylsulfide in the Southern Ocean: Measurements from SO GasEx compared to temperate and tropical regions, Journal of Geophysical Research: Oceans, 116, C00F05, doi:10.1029/2010JC006526, 2011.

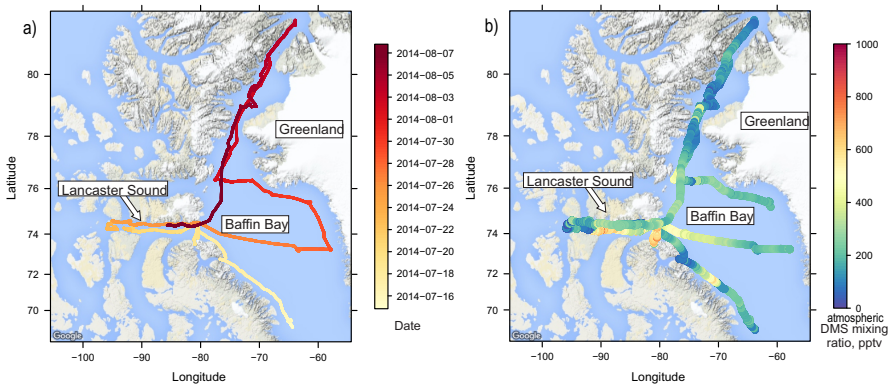

Figure 1. a) The *Amundsen* ship position with dates indicated by colours. b) Surface-layer atmospheric dimethyl sulfide (DMS) mixing ratios from ship-based high resolution time of flight chemical ionization mass spectrometer (HR-ToF-CIMS) measurement with colour showing magnitude of mixing ratios.

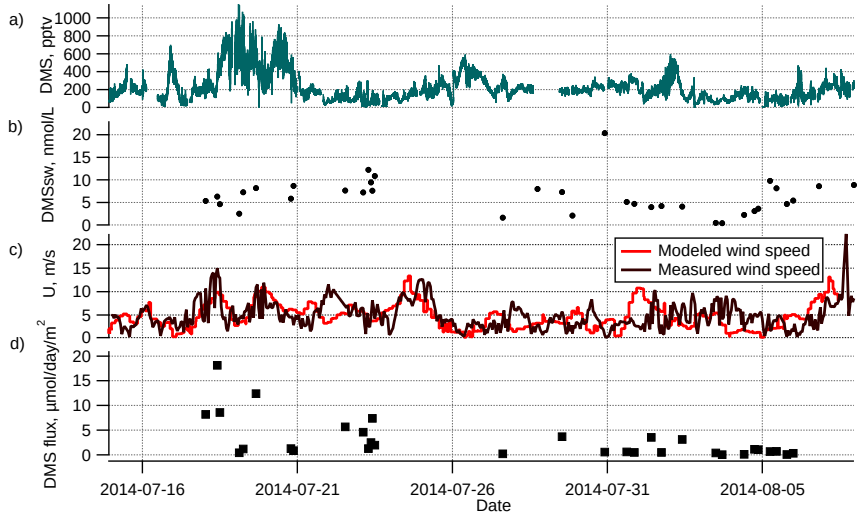

Figure 2. Time series along *Amundsen* ship track of a) atmospheric DMS mixing ratio (10 Hz) from HR-ToF-CIMS, b) observed DMS surface seawater concentration, c) hourly-averaged wind speed at ship position (black) and hourly-average GEOS wind speed at ship position (red), d) DMS water-air flux estimates

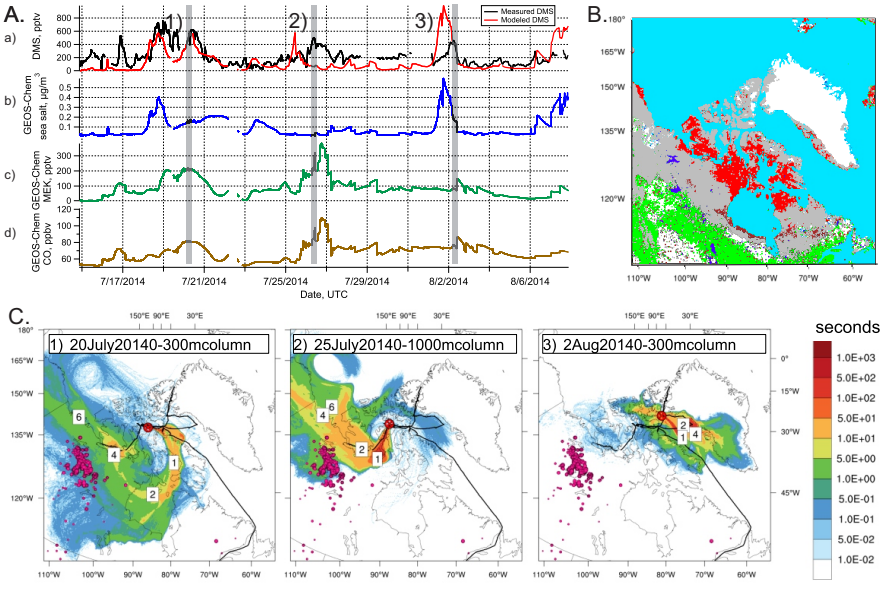

Figure 3. Panel A) Surface-layer atmospheric time series along *Amundsen* ship track of a) measured and GEOS-Chem (GC) simulated DMS, b) GC simulation of accumulation mode sea salt mass concentration, c) GC simulation of methyl ethyl ketone (MEK) mixing ratio, d) GC simulation of carbon monoxide (CO) mixing ratio. Panel B) Olson Land Cover map of North America showing low-lying tundra (red), other tundra (gray), forest (green), wetlands and marsh (brown) and inland water (dark blue). Panel C) FLEXPART-WRF potential emissions sensitivity (PES) simulation plots showing the likely origin of the air mass at the ship position. The colour scale in seconds corresponds to time spent in the lower 300-1000 m (marked on each plot) before arriving at the ship position. The three plots correspond to the three periods shown by the numbers and shaded bars in Panel A, showing examples of 1) transport from lower latitudes, including Hudson Bay 2) continentally influenced air 3) local marine influence from Baffin Bay.

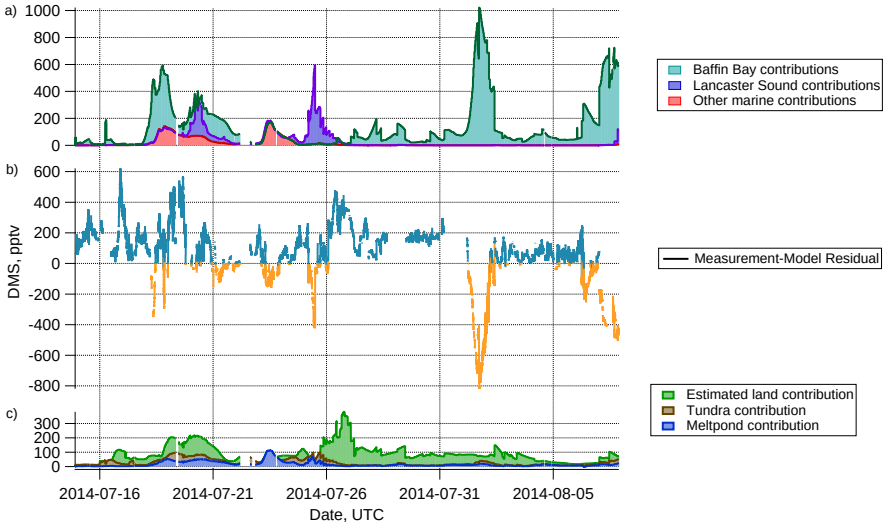

Figure 4. a) GEOS-Chem (GC) simulated atmospheric surface-layer DMS mixing ratio along *Amundsen* ship track as in Fig. 3A, with indication of contributions from Baffin Bay (blue), from Lancaster Sound (purple), and from other marine regions (red). b) Difference between measurement and simulated DMS mixing ratio time series along the ship track showing model over prediction in blue and under prediction in orange. c) GC simulated DMS contributions along ship track from sensitivity tests for additional DMS sources such as melt ponds (blue), tundra (brown), and unknown sources possibly including forests, soils, or lakes in proximity to biomass burning (green).

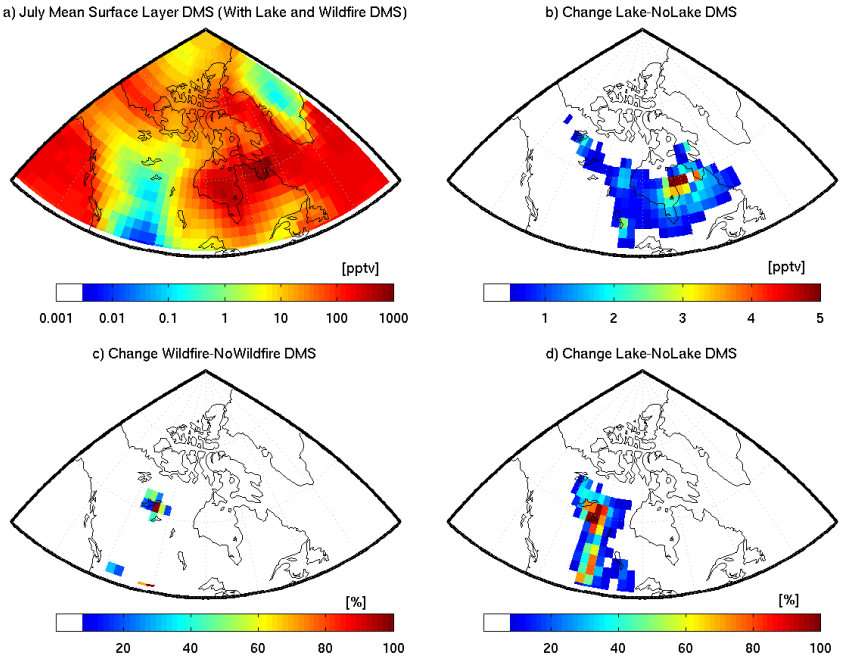

Figure 5. a) GEOS-Chem simulated July mean surface-layer atmospheric DMS in Canada, b) absolute change in simulated surface layer DMS with implementation of lake DMS emissions, c) percent change in simulated Canadian surface layer DMS due to DMS emissions from wildfires, d) percent changes in simulated surface layer DMS with the implementation of lake DMS emissions.

Table 1. Summary of past DMS atmospheric mixing ratio measurements in the Arctic

Study	Leck and Persson (1996)	Rempillo et al. (2011)	Rempillo et al. (2011)	Chang et al. (2011)	Tjernström et al. (2014)	This Work
Cruise Name	IAOE-91	Amundsen 2007	Amundsen 2008	Amundsen 2008	ASCOS 2008	Amundsen 2014
Season	Fall (August, September, October)	Fall (Early October)	Fall (Late September)	Fall (End of August, September)	Fall (August, beginning of September)	Summer (Late July and Early August)
Location	Central Arctic Ocean	Western Canadian Arctic	Eastern Canadian Arctic	Eastern Canadian Arctic	Central Arctic Ocean	Eastern Canadian Arctic
Method	Gas chromatography	Gas chromatography	Gas chromatography	Proton Transfer Reaction Mass Spectrometry	Proton Transfer Reaction Mass Spectrometry	Benzene Chemical Ionization Mass Spectrometry
Measurement Frequency	392 samples in 64 days	9 samples in 3 days	18 samples in 3 days	5 min	1 min	10 Hz
Median	25 (1.1)	10 (0.44)	30 (1.3)	65.9	26	185.8
25th percentile	11 (0.48)			41.2	15	117.8
75th percentile	53 (2.3)			98.9	50	262.5
Minimum	1.1 (0.047)	Below detection (<7 pptv)	Below detection (<7 pptv)	0.3	4.0	Below detection (<4 pptv)
Maximum	380 (17)	30 (1.3)	94 (4.1)	474	158	1155

The studies of Leck and Persson (1996) and Rempillo et al. (2011) report concentrations in nmol/m^3. For purposes of comparison, these have been converted to mixing ratios for an atmospheric pressure and temperature of 101 kPa and 4 ^{circ} respectively. Original (published) concentration values are reported in parentheses following the calculated mixing ratios.

Table 2. Summary of previous air-ocean DMS flux values in the Arctic

Flux	**Date**	**Location**	**Method**	**Authors**
0.02-12 μmol m^{-2}d^{-1}	Summer 2014 (July and August)	Eastern Canadian Arctic	Estimated from measurements	This work
0.1-2.6 μmol m^{-2}d^{-1}	Fall 2007, 2008 (September to November)	Beaufort Sea to Baffin bay through Lancaster Sound	Estimated from measurements	(Rempillo et al., 2011)
0.002-8.4 μmol m^{-2}d^{-1}	Fall 1991 (August to October)	Central Arctic Ocean and Greenland Sea	Estimated from measurements	(Leck and Persson, 1996)
0.007-11.5 μmol m^{-2}d^{-1}	Summer 1994 (July and August)	Central Arctic Ocean East-West transect	Estimated from measurements	(Sharma et al., 1999b)
0.5 μmol m^{-2}d^{-1}	January	North of 60°N	Global model	(Erickson et al., 1990)
4-12 μmol m^{-2}d^{-1}	March-December 1996	Gulf of Alaska	Regional Model	(Jodwalis et al., 2000)